Remote Sensing of Environment 140 (2014) 279–293

Contents lists available at ScienceDirect

Remote Sensing of Environment

journal homepage: www.elsevier.com/locate/rse

Comparison of satellite-based evapotranspiration models over terrestrial ecosystems in China

Yang Chen [a,b], Jiangzhou Xia [a,b], Shunlin Liang [b,c], Jinming Feng [a,d], Joshua B. Fisher [e], Xin Li [f], Xianglan Li [b], Shuguang Liu [g], Zhuguo Ma [d], Akira Miyata [h], Qiaozhen Mu [i], Liang Sun [j], Jianwei Tang [k], Kaicun Wang [a,b], Jun Wen [f], Yueju Xue [l], Guirui Yu [m], Tonggang Zha [n], Li Zhang [o], Qiang Zhang [k], Tianbao Zhao [d], Liang Zhao [p], Wenping Yuan [a,q,*]

[a] State Key Laboratory of Earth Surface Processes and Resource Ecology, College of Global Change and Earth System Science, Beijing Normal University, Beijing 100875, China
[b] State Key Laboratory of Remote Sensing Science, Jointly Sponsored by Beijing Normal University and Institute of Remote Sensing Applications, Chinese Academic of Science, Beijing 100875, China
[c] Department of Geographical Sciences, University of Maryland, College Park, MD 20742, USA
[d] Key Laboratory of Regional Climate-Environment Research for Temperate East Asia, Institute of Atmospheric Physics, Chinese Academy of Sciences, Beijing 100029, China
[e] Jet Propulsion Laboratory, California Institute of Technology, Pasadena, CA 91109, USA
[f] Cold and Arid Regions Environmental and Engineering Research Institute, Chinese Academy of Sciences, Lanzhou, Gansu 730000, China
[g] State Engineering Laboratory of Southern Forestry Applied Ecology and Technology, Central South University of Forestry and Technology, Changsha, Hunan 410004, China
[h] National Institute for Agro-Environmental Sciences, Tsukuba 305-8604, Japan
[i] College of Forestry & Conservation, The University of Montana, Missoula, MT 59812, USA
[j] Institute of Agricultural Resources and Regional Planning, Chinese Academy of Agricultural Sciences, Beijing 100081, China
[k] Meteorological Bureau of Gansu Province, Lanzhou, Gansu 730000, China
[l] College of Information, South China Agricultural University, Guangzhou 510642, China
[m] Key Laboratory of Ecosystem Network Observation and Modeling, Synthesis Research Center of Chinese Ecosystem Research Network, Institute of Geographic Sciences and Natural Resources Research, Chinese Academy of Sciences, Beijing 100101, China
[n] School of Resources and Environment, Beijing Forestry University, Beijing 100083, China
[o] Center for Earth Observation and Digital Earth, Chinese Academy of Sciences, Beijing 100094, China
[p] Key Laboratory of Qinghai-Tibetan Plateau Biological Evolution and Adaptation, Northwest Institute of Plateau Biology, The Chinese Academy of Sciences, Xining, Qinghai 810008, China
[q] State Key Laboratory of Cryosphere Sciences, Cold and Arid Regions Environmental and Engineering Research Institute, The Chinese Academy of Sciences, Lanzhou, Gansu 730000, China

ARTICLE INFO

Article history:
Received 30 January 2013
Received in revised form 30 August 2013
Accepted 31 August 2013
Available online xxxx

Keywords:
Evapotranspiration
Eddy covariance
Priestley–Taylor
Penman–Monteith

ABSTRACT

Evapotranspiration (ET) is a key component of terrestrial ecosystems because it links the hydrological, energy, and carbon cycles. Several satellite-based ET models have been developed for extrapolating local observations to regional and global scales, but recent studies have shown large model uncertainties in ET simulations. In this study, we compared eight ET models, including five empirical and three process-based models, with the objective of providing a reference for choosing and improving methods. The results showed that the eight models explained between 61 and 80% of the variability in ET at 23 eddy covariance towers in China and adjacent regions. The mean annual ET for all of China varied from 535 to 852 mm yr^{-1} among the models. The interannual variability of yearly ET varied significantly between models during 1982–2009 because of different model structures and the dominant environmental factors employed. Our evaluation results showed that the parameters of the empirical methods may have different combination because the environmental factors of ET are not independent. Although the three process-based models showed high model performance across the validation sites, there were substantial differences among them in the temporal and spatial patterns of ET, the dominant environment factors and the energy partitioning schemes. The disagreement among current ET models highlights the need for further improvements and validation, which can be achieved by investigating model structures and examining the ET component estimates and the critical model parameters.

1. Introduction

Evapotranspiration (ET), which is the water transferred from land to the atmosphere via surface evaporation and plant transpiration, links the terrestrial water, carbon, and surface energy exchanges (Wang & Dickinson, 2012). It provides the atmospheric moisture that eventually

* Corresponding author at: State Key Laboratory of Earth Surface Processes and Resource Ecology, College of Global Change and Earth System Science, Beijing Normal University, Beijing 100875, China. Tel.: +86 10 58807715.
E-mail address: wenpingyuancn@yahoo.com (W. Yuan).

0034-4257/$ – see front matter © 2013 Elsevier Inc. All rights reserved.
http://dx.doi.org/10.1016/j.rse.2013.08.045

returns to the surface as rain or snow and also consumes an enormous amount of heat, which helps to cool the land surface (Bonan, 2008). Therefore, accurate knowledge of the temporal and spatial variations in ET is critical for understanding the interactions between land surfaces and the atmosphere (Keane et al., 2002; Kustas & Norman, 1996), improving water resource management (Meyer, 1999; Raupach, 2001) and for investigating drought occurrence and impact (McVicar & Jupp, 1998). However, ET remains the most problematic component of the water cycle because of the heterogeneity of the landscape and the large number of controlling factors involved, including climate, plant biophysics, soil properties, and topography (Friedl, 1996; Gash, 1987; Lettenmaier & Famiglietti, 2006).

Recently, numerous methods have been developed to estimate terrestrial ecosystem ET, but inter-comparisons of global ET estimates have revealed large model uncertainties (Vinukollu, Meynadier, Sheffield, & Wood, 2011). The results of the Global Soil Wetness Project-2 (GSWP-2) showed that mean annual global ET ranged from 272 to 441 mm yr^{-1} among 15 models, and the maximum estimate was 1.5 times the minimum (Dirmeyer et al., 2006). Similarly, large differences in global ET simulations have also been found among six common land models and five global hydrological models, with values ranging from 415 to 586 mm yr^{-1} (Haddeland et al., 2011). Moreover, the uncertainties in global land ET from multiple remote sensing methods, land surface models (LSMs) and reanalysis, are close to 50% of total annual mean values (Jiménez et al., 2011; Mueller et al., 2011).

Satellite-based observations of land surface and atmospheric properties provide the most spatiotemporally consistent and direct estimates of land surface properties (Jiménez, Prigent, & Aires, 2009), if used appropriately in physically accurate and statistically robust models (Liang, Li, & Wang, 2012). Some physical process ET models have been developed based on the Penman–Monteith (Cleugh, Leuning, Mu, & Running, 2007; Monteith, 1965; Mu, Heinsch, Zhao, & Running, 2007; Mu, Zhao, & Running, 2011; Yuan et al., 2010) or Priestley–Taylor equations (Fisher, Tu, & Baldocchi, 2008; Miralles et al., 2011). However, some of the process-based ET models are limited by their requirements for extensive parameterizations of highly variable factors such as maximum stomatal conductance and soil water content (Yang et al., 2006). The relatively large uncertainties in these models pose a challenge for the accurate assessment of ET. Therefore, empirical regression models have been used to upscale eddy covariance measurements (Jung et al., 2010; Papale & Valentini, 2003; Yang et al., 2007; Zhou et al., 2008).

All ET models come with simplifying assumptions, and have different formulations of the processes that control the land–atmosphere water flux. There is diversity in both the complexity of model structures and their formulation, often because they were designed for different applications or purposes. The result is a wide range of estimates of regional ET. Each model, therefore, is a combination of scientific hypotheses and choices, and its formulation depends on the inherent assumptions, driving data and parameter values. With the relatively recent advent of available local observations of ET fluxes from eddy covariance, as well as advances in our current understanding of the processes controlling ET over regional scales, we can start to determine which model is "best" at representing current fluxes, though by no means are the available data sufficient to definitively answer that question. Nevertheless, to move towards more robust estimates of ET dynamics, it is necessary to compare estimates from a variety of model types, as well as to evaluate estimates against the measurements that are available (Vinukollu, Wood, Ferguson, & Fisher, 2011). Although it is a challenge to interpret the internal mechanisms that cause the differences in ET estimates, there is also great value in using independent estimates to identify their advantages, disadvantages, and uncertainties. However, most previous analyses were of limited spatial, temporal coverage (Bormann, 2010; Li, Kang, Li, & Zhang, 2008; Su, McCabe, Wood, Su, & Prueger, 2005; Werth & Avissar, 2004; Wilson, Hanson, Mulholland, Baldocchi, & Wullschleger, 2001; Zhang, Kang, Li, & Zhang, 2008).

In this study, we compared eight ET models, including five empirical models and three process-based models, using the ET measurements at twenty-three eddy covariance sites within or around China. The primary objectives of this study are to (1) compare the performance of eight ET models based on the ET observations; (2) assess the differences in the temporal and spatial patterns of ET over China during 1982–2009; (3) investigate the dominant environment variables of ET models; and (4) analyze differences of model structure.

2. Methods and data

2.1. Evapotranspiration models

We examined five empirical models and three process-based models in this study. The five empirical models include an artificial neural network (ANN) model (Papale & Valentini, 2003), a regression tree (RT) model (Zhang et al., 2007), a support vector model (SVM, Yang et al., 2006) and two regression models (Reg1 and Reg2) developed by Wang, Wang, Li, Cribb and Sparrow (2007), and Wang, Dickinson, Wild and Liang (2010). The three process-based models include two Penman–Monteith type models (i.e., PM–MOD16 algorithm, Mu et al., 2011; PM–Yuan model, Yuan et al., 2010) and one Priestley–Taylor type model (PT–JPL, Fisher et al., 2008).

The ANN is composed of several elements called neurons or nodes. The basic structure of a network consists of three layers: input layer, hidden layer and output layer. The ANN adjusts the weight of internal nodes with training data. We used the back propagation artificial neural network which was developed by Rumelhart, Hinton, and Williams (1986) to find the best fit with the training data. The multilayer perceptron (MLP), the most common and widely used feed-forward network, was applied in this study. The ANN can represent any arbitrary nonlinear function given sufficient complexity of the trained network, and it can find relationships between different input samples. Most importantly, the ANN is able to generalize a relationship from small subsets of the data while remaining relatively robust in the presence of noisy or missing inputs, and can adapt or learn in response to changing environments (Dawson & Wilby, 1998).

Regression tree (RT) algorithms typically predict class membership by recursively partitioning a dataset into a more homogeneous membership (Xiao et al., 2010). RT models can account for a nonlinear relationship between predictive and target variables and allow both continuous and discrete variables. We used a modified regression tree algorithm implemented in the commercial software called Cubist (RuleQuest Research. Pty Ltd Company, 30 Athena Avenue, St Ives, NSW 2075, Australia), which is a powerful tool for generating rule-based predictive models.

Support vector machine (SVM) is a supervised non-parametric statistical learning technique. SVM can transform nonlinear regressions into linear regressions by converting the low dimensional input space into a higher dimensional feature space (Vapnik, 1998). It is widely used to approximate regressions due to its ability to approximate any nonlinear functions, especially when samples are limited. In previous studies, SVM has been used to estimate many parameters, such as wind speed, precipitation, ecological niches and evapotranspiration (Drake, Randin, & Guisan, 2006; Mohandes, Halawani, Rehman, & Hussain, 2004; Tripathi, Srinivas, & Nanjundiah, 2006; Yang et al., 2006).

The Reg1 model estimates ET using surface net radiation, air temperatures and a vegetation index as the dominant variables controlling evapotranspiration (Wang et al., 2007). It expresses the dependence of ET variations on the vegetation in the simplest form that is consistent with the Priestley–Taylor equation while incorporating the influence on vegetation control on ET. This method has been used to predict ET under a wide range of soil moisture contents and land cover types (Wang et al., 2007).

The Reg2 model divides ET into energy control (ET_e) and the atmospheric control (ET_a) components (Wang et al., 2010). A regression

was used to determine ET_e and ET_a based on remote sensing and eddy covariance flux data. This method adds empirical coefficients to a Penman-based equation to include dependence on vegetation and soil moisture. This allows ET to be estimated over a wide range of climate conditions. This simple but accurate method can investigate decadal variation in regional ET over the land (Wang et al., 2010). The Reg2 model uses surface net radiation, air temperature, wind speed and a vegetation index as the model forcing data.

The first process-based algorithm (PT–JPL) was developed by Fisher et al. (2008) based on the Priestley and Taylor (1972) equation, with dynamic coefficients estimated from atmospheric moisture and vegetation indices to downscale potential ET to actual ET. The total ET is calculated as the sum of ET_c (canopy transpiration), ET_s (soil evaporation) and ET_i (interception evaporation). Each component is calculated with the Priestley–Taylor equation and the corresponding ecophysiological constraints.

The second process-based algorithm (PM–MOD16) was developed by Mu et al. (2011) based on the Penman–Monteith equation (Monteith, 1965) and as adapted by Cleugh et al. (2007). Mu et al. included a soil evaporation component, using moisture and temperature constraints on stomatal conductance, and inferring canopy conductance from the leaf area index. Mu et al. (2011) further modified the ET algorithm by 1) simplifying the calculation of vegetation cover fraction; 2) calculating ET as the sum of daytime and nighttime components; 3) adding soil heat flux calculation; 4) improving estimates of stomatal conductance, aerodynamic resistance and boundary layer resistance; 5) separating dry canopy surface from the wet; and 6) dividing the soil surface into saturated wet and moist surfaces. Model validation at 46 eddy flux towers showed that the improved algorithm enhanced accuracy (Mu et al., 2011).

The third process-based algorithm (PM–Yuan) is also a Penman–Monteith type model as modified by Yuan et al. (2010). In the PM–Yuan model, the temperature constraint for stomatal conductance follows the equation detailed by June, Evans, and Farquhar (2004) and in PT–JPL from Fisher et al. (2008). The Beer–Lambert law is used to exponentially partition net radiation between the canopy and the soil surface (Ruimy, Kergoat, Bondeau, & intercomparison, 1999). This method improved the ET estimates at most of the 54 flux towers compared with the ET estimates of the original RS–PM algorithm (Yuan et al., 2010).

2.2. Data at eddy covariance sites

Measurements of eddy covariance (EC) were used to examine model performance. Twenty-three EC sites, from ChinaFlux, AsiaFLUX, LathuileFLUX and Arid/Semi-arid experimental observation synergy and integration (Guan, Huang, Guo, Bi, & Wang, 2009; Huang, Guan, & Ji, 2012; Huang et al., 2008; Li et al., 2009; Zhang, Zeng, & Yao, 2012), were included in this study (Fig. 1). The sites covered seven major terrestrial biomes: deciduous broadleaf forests (DBF), mixed forests (MF), evergreen needleleaf forests (ENF), evergreen broadleaf forests (EBF), deciduous needleleaf forests (DNF), grasslands (GRA) and croplands (CRO). Daily solar radiation (R_g), net radiation (R_n), air temperature (T_a), relative humidity (R_h), wind speed (W_s), atmospheric pressure (P), vapor pressure deficit (VPD) and site elevation were used to drive the models.

It has been noted that the sum of sensible heat (H) and latent heat (LE) as measured by the EC method is generally less than the available energy (Foken, 2008). Assuming that the ratio of sensible heat to ET is correct, LE measurements can be corrected as follows (Jung et al., 2010):

$$LE_{cor} = (R_n - G)/(H_{uncor} + LE_{uncor}) \times LE_{uncor} \quad (1)$$

where LE_{cor} is the corrected latent heat, R_n is the net radiation, G is the soil heat flux, H_{uncor} is the uncorrected sensible heat and LE_{uncor} is the uncorrected latent heat. The results showed that energy closure was improved 18–48% after this correction (data not shown).

Normalized difference vegetation index (NDVI) and leaf area index (LAI) for the EC towers were determined from the Moderate Resolution Imaging Spectroradiometer (MODIS). MODIS ASCII data were used in this study and generated from MODIS Collection 5 data, which were downloaded directly from the Oak Ridge National Laboratory Distributed Active Center (ORNL DAAC) web site (http://daac.ornl.gov/MODIS/). The 8-day MODIS LAI (MOD15A2) and 16-day MODIS NDVI (MOD13A2) data at 1 × 1 km spatial resolution were the basis for model verification in the flux sites. Only the NDVI and LAI values of

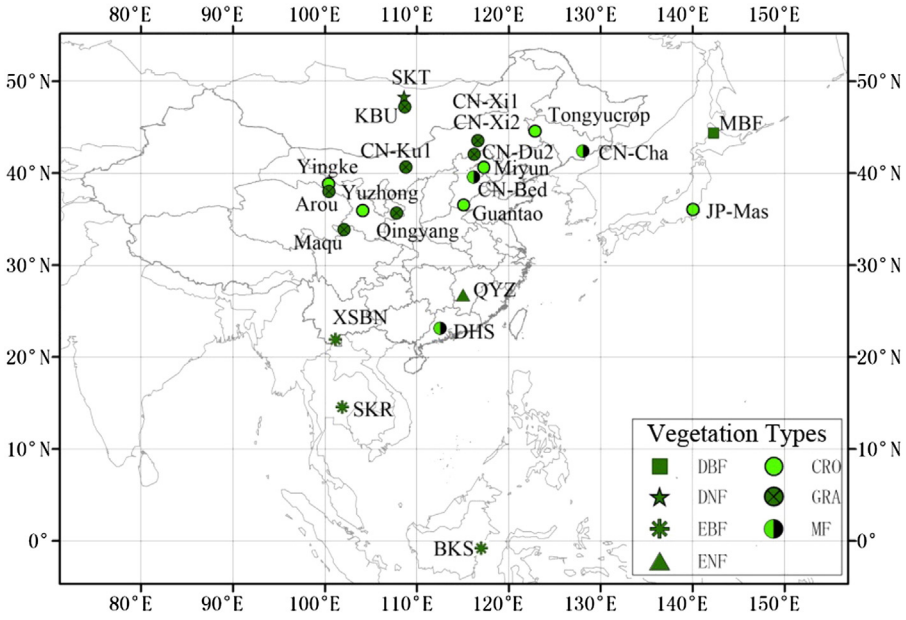

Fig. 1. Names, locations and vegetation types of the twenty-three EC sites. DBF: deciduous broadleaf forests; DNF: deciduous needleleaf forests; EBF: evergreen broadleaf forests; ENF: evergreen needleleaf forests; CRO: croplands; GRA: grasslands; MF: mixed forests.

the pixels containing the tower were used. Quality control (QC) flags, which signal cloud contamination in each pixel, were examined to screen and reject poor quality NDVI and LAI data.

2.3. Data at regional scale

When estimating ET at the regional scale for all eight models, we used datasets for monthly total radiation (R_g), net radiation (R_n), air temperature (T_a), relative humidity (R_h), wind speed (W_s), and air pressure (P) from the MERRA (Modern Era Retrospective-Analysis for Research and Applications) archive for 1982–2009 (Global Modeling & Assimilation Office, 2004). MERRA is a NASA reanalysis for the satellite era that uses a new version of the Goddard Earth Observing System Data Assimilation System Version 5 (GEOS-5). The MERRA reanalysis dataset has been validated at the global scale using surface meteorological data to evaluate the uncertainty of various meteorological factors (i.e., temperature, radiation, humidity, and energy balance) (Global Modeling & Assimilation Office, 2004). Compared with previous reanalyses, such as Clouds and the Earth's Radiant Energy System (CERES), NCEP/NCAR Reanalysis 1 (NCEP1), NCEP-DOE AMIPII Reanalysis (NCEP2), ECMWF 40 Year Re-analysis (ERA-40) and the Japanese 25-year Reanalysis (JRA-25) and North American Regional Reanalysis (NARR), MERRA showed comparable results for the global water and energy cycle (Chen & Bosilovich, 2008; Kennedy, Dong, Xi, Xie, & Chen, 2011). Detailed information on the MERRA dataset is available at the NASA website (http://gmao.gsfc.nasa.gov/research/merra).

We used the AVHRR and MODIS LAI and NDVI datasets to generate the combined LAI and NDVI from 1982 to 2009. The AVHRR GIMMS NDVI is based on a composite of monthly maximum values of biweekly data with a 0.0727 degree spatial resolution and covers the period from 1982 to 2006. We used maximum value composite to minimize atmospheric and cloud contamination effects on NDVI data (Holben, 1986). Global 8-day MODIS NDVI (MOD13A2) data were used and aggregated into monthly NDVI data. Quality control (QC) flags were examined to screen and reject poor quality NDVI data. We filled in the missing or unreliable NDVI at each 1-km MODIS pixel based on their corresponding quality assessment data fields as proposed by Zhao, Heinsch, Nemani, and Running (2005). To be consistent with the spatial resolution of the AVHRR NDVI data, MODIS NDVI data were first spatially aggregated to a resolution of approximately 0.0727°. The following procedures were then used to combine the two series (Zhang, Kimball et al., 2008): (1) regress monthly MODIS NDVI on corresponding AVHRR NDVI for the overlapping period from 2000 to 2006 using simple linear regression on a pixel-by-pixel basis; (2) use the resulting regression equations to adjust the AVHRR NDVI time series and compute an integrated AVHRR–MODIS NDVI monthly time series from 1982 to 2006. Similarly, 8-day MODIS LAI (MOD15A2) (Myneni et al., 2002) and monthly AVHRR LAI (Myneni, Nemani, & Running, 1997) were used in this study, and the same procedures were implemented to generate a continuous LAI dataset for 1982–2009. The spatial resolution of all the forcing data and the model simulations is 0.1°, covering the terrestrial ecosystem area of China as defined by the MODIS Land Cover product (MOD12Q1).

2.4. Statistical analysis

A linear trend analysis was used to analyze regional trends in ET and meteorological and vegetation variables (y_t) using a linear model ($y_t = bx_t + y_0$, Zhang et al., 2009), where t, b and y_0 are the time, slope and intercept of the regression line, respectively. The statistic $b/SE(b)$ (where $SE(b)$ is the standard deviation of b) has Student's t-distribution, and Student's t-test was used to analyze and classify the significance of the trend as 'weak', 'moderate', or 'strong'. When $|b/SE(b)| < 1.0$, i.e., b is within one standard deviation, the trend is classified as weak; when $1.0 \le |b/SE(b)| \le t_{0.10}$ where $t_{0.10}$ is the 10% critical value of Student's t-distribution, the trend is classified as moderate; when $|b/SE(b)| \ge t_{0.10}$, the trend is statistically significant and classified as strong. These categories were further stratified into six classes according to the slopes of the statistical trends: positive weak, positive moderate, positive strong, negative weak, negative moderate, and negative strong.

The following metrics were used to evaluate model performance in this study. The coefficient of determination (R^2) represented how much variation in the observations was explained by the model. The root mean square error (RMSE) was used to quantify the difference between simulated and observed values. The Kling–Gupta efficiency (KGE,

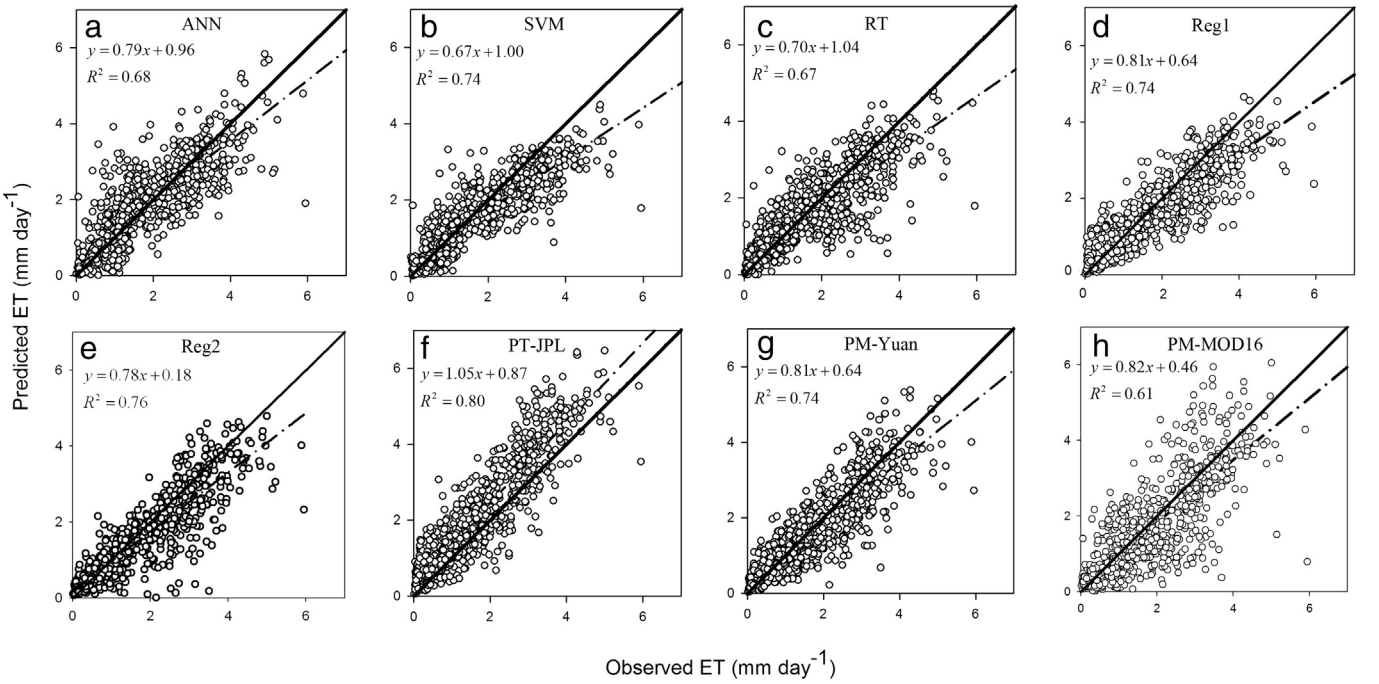

Fig. 2. Observed evapotranspiration (ET) at eddy covariance sites versus predicted ET from eight models. The solid line is the 1:1 line and the short dashed lines are the regression lines.

Gupta, Kling, Yilmaz, & Martinez, 2009) was used to comprehensively evaluate the model performance. The KGE accounts for the correlation, variability error and bias error and incorporates these criteria into a single multi-objective criterion, and is calculated as follows:

$$\mathrm{KGE} = 1 - ED \tag{2}$$

$$ED = \sqrt{(r-1)^2 + (\alpha-1)^2 + (\beta-1)^2} \tag{3}$$

$$\alpha = \sigma_s/\sigma_o \tag{4}$$

$$\beta = \mu_s/\mu_o \tag{5}$$

where ED is the Euclidian distance from the ideal point, r is the linear correlation coefficient between simulated and the observed values, μ_o and σ_o are the mean and standard deviation of the observations, μ_s and σ_s are the mean and standard deviation of the simulations, α is a measure of relative variability in the simulated and observed values,

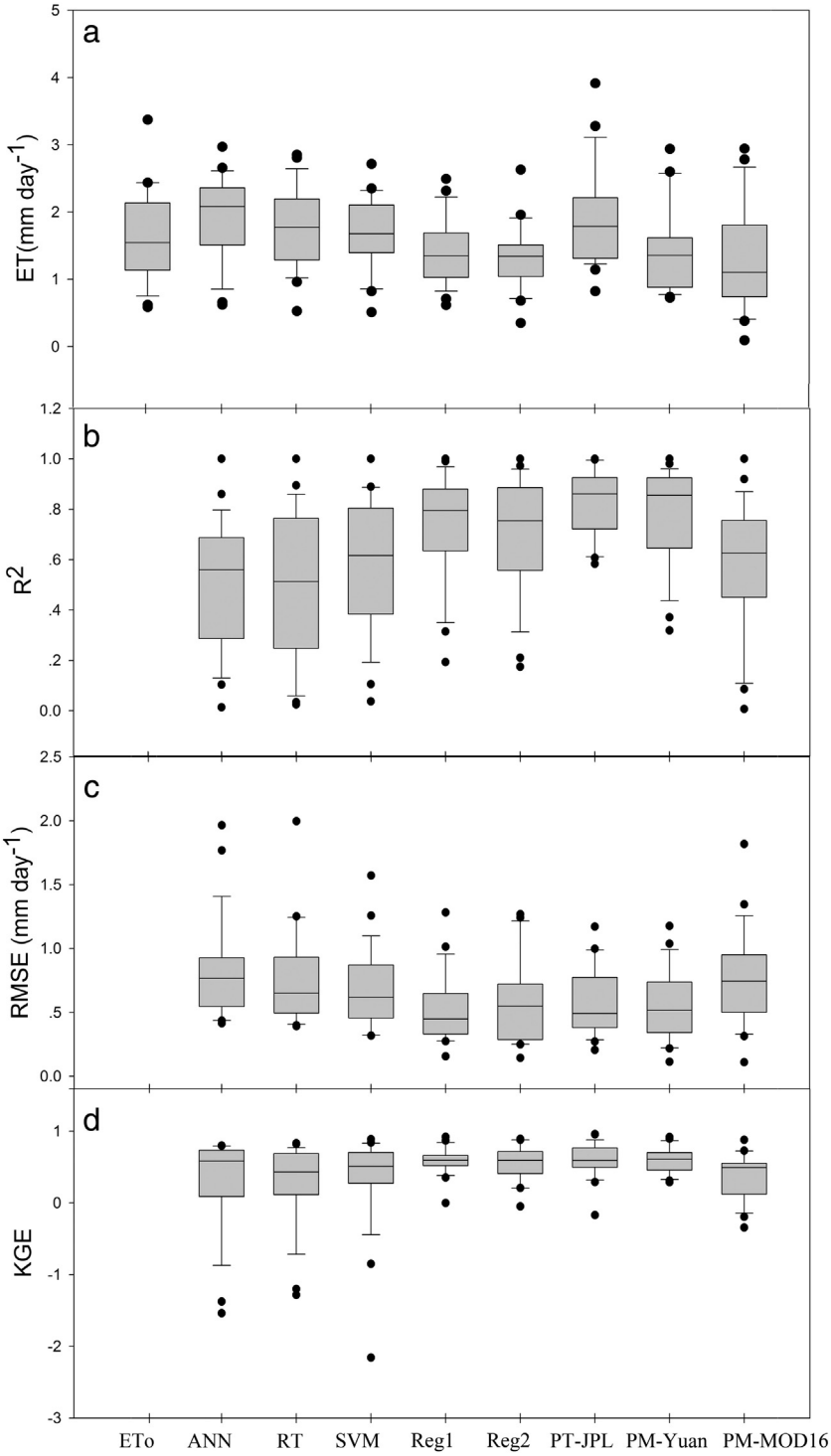

Fig. 3. Comparison of ET observations (ET_o) and simulations of eight models at 23 EC sites: mean values (a), model determination coefficient (R^2) (b), root mean square error (RMSE) (c) and the Kling–Gupta efficiency (KGE) (d).

Table 1
Relationship between the performances of three advanced statistical models with the quantity of training data.

Data rate	RT		SVM		ANN	
	RMSE (mm day^{-1})	R^2	RMSE (mm day^{-1})	R^2	RMSE (mm day^{-1})	R^2
20%	0.86	0.53	0.97	0.52	2.22	0.16
40%	0.76	0.62	0.86	0.55	0.94	0.49
60%	0.69	0.69	0.85	0.56	1.25	0.32
80%	0.70	0.68	0.86	0.59	0.81	0.58
100%	0.71	0.67	0.66	0.74	1.77	0.68

Data rate: the fraction of selected training data to all original training data.

and β is the ratio of the mean values of simulations and observations. The values of the three components are $r = 1$, $\alpha = 1$ and $\beta = 1$ without any simulation errors. Therefore the 'ideal' KGE value is 1.

2.5. Model calibration and experiments with empirical models

In this study, we used three machine learning methods (ANN, SVM and RT). To train these three models, we randomly selected half of the measurements from all sites (738 data samples) and used the other half of the measurements for model validation. To examine the impacts of parameter calibration on model performance, we used the same datasets to recalibrate parameters and validate the two regression models (i.e., Reg1 and Reg2).

3. Results

3.1. Model validation

At the site scale, the model performance differed substantially among the eight models. Generally, the eight models explained 61–80% of ET variability over all measurements (Fig. 2). PT–JPL showed the highest coefficient of determination ($R^2 = 0.80$), followed by Reg2, Reg1, SVM and PM–Yuan with R^2 values ranging from 0.74 to 0.76. Except for the PT–JPL model, all models slightly underestimated the measurements (Fig. 2). The averaged ET simulations of SVM, Reg1, Reg2, PT–JPL and PM–Yuan were very similar to the observations (Fig. 3a). At the individual sites, the Reg1, Reg2, PT–JPL and PM–Yuan presented higher R^2 values and a lower RMSE than others (Fig. 3b, c). Although the KGE median values for all models were close (Fig. 3d), ANN, RT, SVM and PM–MOD16 showed large differences among sites, which implied inconsistent model performance over the study sites. Overall, according to KGE values, the performances of Reg1, Reg2, PT–JPL and PM–Yuan were better (Fig. 3d).

The three advanced statistical models (ANN, SVM and RT) had the poorest performance, and the average R^2 values of these models over 23 EC sites were 0.68, 0.74 and 0.67, respectively (Table 1). In general, the performance of the statistical models strongly depended on the quantity and representativeness of the training datasets. To examine the impacts of training datasets, we conducted a series of model experiments by changing the quantity of training data. We randomly selected 20, 40, 60 and 80% measurements from the original training datasets to conduct model trainings, and used the original validation datasets. The results showed that model performance decreased significantly with fewer training samples (Table 1). For example, SVM explained 74% of the variability in ET using full training dataset, but only 52% of the variability using the 20% training dataset (Table 1).

Similarly, the performance of the two other empirical models (Reg1 and Reg2 models) was also highly related to the regression coefficients. For example, the original parameters of Reg1 were calibrated over the Southern Great Plains (SGP) area of the United States, and the parameter values of a_0, a_1 and a_2 were set as 0.1505, 0.45 and 0.004, respectively (Wang et al., 2007). When the three parameters were recalibrated in this study, the parameter values increased to 0.1077, 0.395 and 0.0104. Accordingly, the annual mean ET changed to 673 mm yr^{-1} as opposed to the 559 mm yr^{-1} derived using the original model parameters (Fig. 4). This is likely because Wang et al. (2007) did not fully consider the impact of soil moisture on ET, which has been improved (Wang & Liang, 2008).

3.2. Spatial and temporal differences in evapotranspiration

All eight models showed similar spatial patterns of ET, with decreasing ET from southeast to northwest China (Fig. 5). The annual mean ET was highest in the humid tropics and sub-tropics, intermediate in temperate regions and the lowest in both cold and arid regions, where either temperature or precipitation was the limiting factors. Comparing the models, however, revealed substantial differences in ET estimates among the eight models, and the mean annual ET over all of China ranged from 535 to 852 mm yr^{-1} among all models. The PT–JPL model simulated the highest ET over nearly all regions. Its mean annual ET was 852 mm yr^{-1} which was 1.59 times the lowest ET estimates from PM–MOD16. Overall, the largest difference in ET estimates occurred in tropical and humid areas with high levels of ET (Fig. 5). All eight models showed strong seasonality in ET (Fig. 6), and they captured the seasonality of averaged ET. All of the models had a similar monthly variation, with maxima in the summer and minima in the winter. However, there was substantial variation in the monthly ET among models.

The long-term changes in ET differed among eight models. Four of eight models (i.e., SVM, Reg1, Reg2 and PM–Yuan) showed a significant increase in ET from 1982 to 2009, with the trends ranging from 0.62 to 2.55 mm yr^{-1}, and the largest increase in ET was found by the SVM model. The other two models presented relatively constant long-term

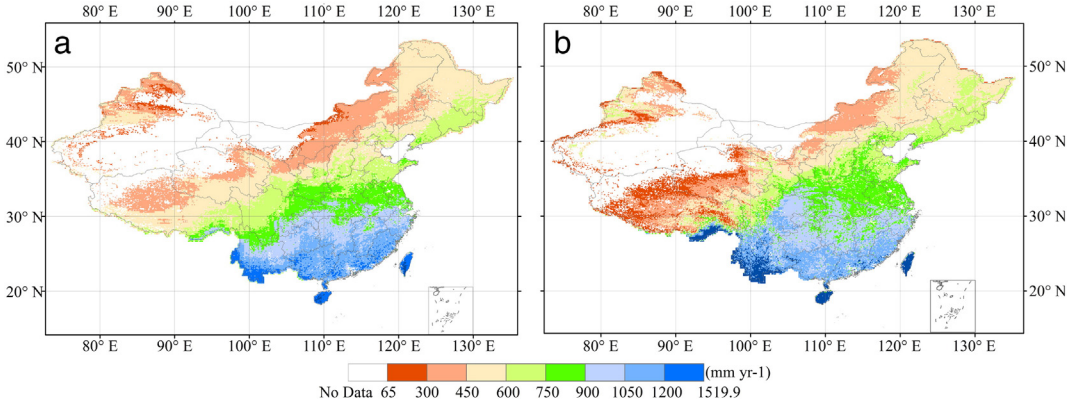

Fig. 4. Spatial patterns of ET simulations derived from Reg1 models with original parameter values (a) and recalibrated parameters (b).

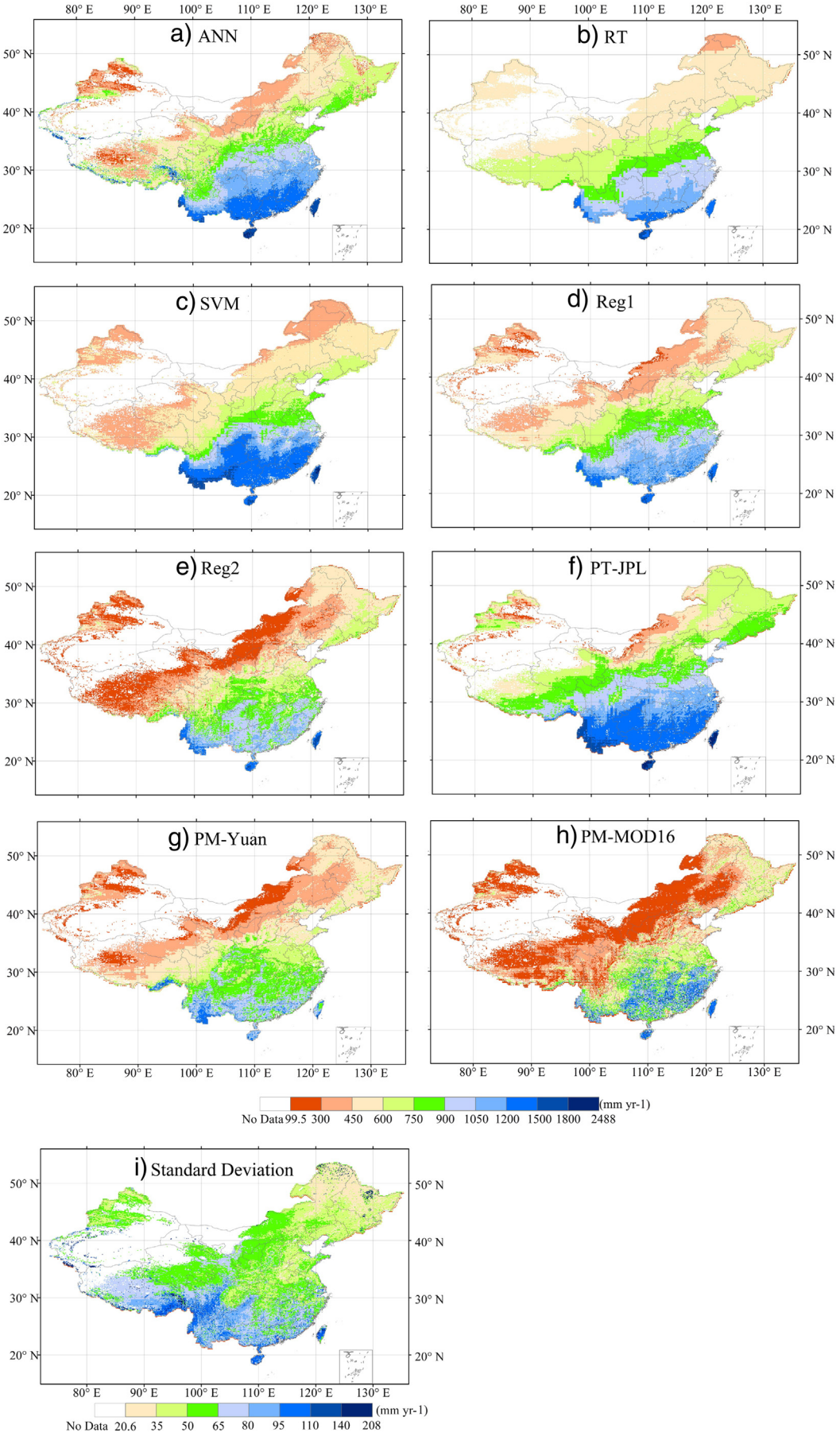

Fig. 5. Spatial patterns of mean annual ET simulations from 1982 to 2009 and standard deviation of mean annual ET from eight models.

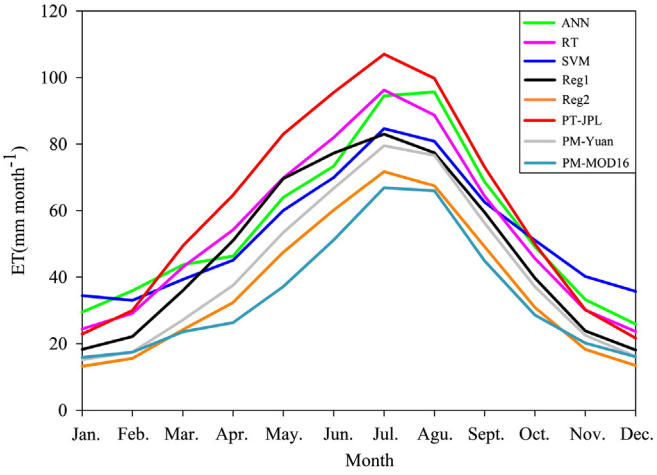

Fig. 6. Seasonal variability of the mean ET simulations from eight models.

change (i.e., RT and PT–JPL), and ANN and PM–MOD16 showed slightly decreased ET (0.16 mm yr^{-1}, p = 0.63 and 0.04 mm yr^{-1}, p = 0.88) (Fig. 7; Table 2). In terms of spatial pattern, the differences in the long-term ET were found over almost the entire territory of China. SVM, RT, Reg1, Reg2, PT–JPL and PM–Yuan had larger areas with strongly increasing ET (Fig. 8). In particular, 89% of the area was dominated by the positive ET trend in Reg1. In contrast, positive trends in ET accounted for approximately 49 and 46% of China according to the PM–MOD16 and ANN models. No consistent ET trends were found among all models throughout China, and only 38% of regions had consistent interannual variability trends in more than 4 models (Fig. 8i). For example, over northern China, Reg1, PM–Yuan and PM–MOD16 simulated strongly positive ET trends (Fig. 8d, g, h); however, the opposite was found in RT, Reg2 and PT–JPL (Fig. 8c, e, f). Relatively consistent change trends were found in southern China, with increased ET indicated by most models (Fig. 8). In northeast China, there were again significant differences in the trends among the models.

The three process-based models simulated the ET components separately. PT–JPL and PM–MOD16 separated ecosystem ET into canopy transpiration (ET_c), soil evaporation (ET_s) and interception evaporation from the wet plant and soil surfaces (ET_i), and the PM–Yuan model only simulated ET_c and ET_s. PT–JPL had the highest simulations of ET_c and ET_s among the three models. In contrast, PM–MOD16 showed the lowest ET_c and ET_s. ET_i estimates from PT–JPL and PM–MOD16 were similar in magnitude and interannual variation (Fig. 9). The long-term trends of the ET components were consistent among the models. In general, all three models showed increased ET_c and decreased ET_s and ET_i. The three ET components showed a relatively consistent trend of decreasing magnitude from south to north (data not shown).

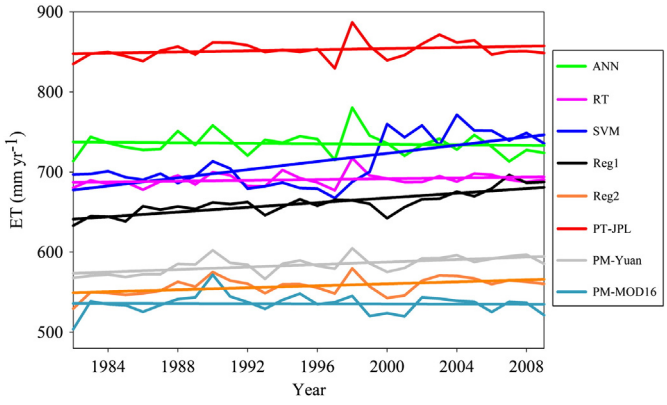

Fig. 7. Interannual variability of the ET simulations of eight models from 1982 to 2009.

Table 2
Long-term change trends of mean annual ET for vegetated land area of China from 1982 to 2009.

Model	a (mm yr^{-1})	b (mm)	p
ANN	−0.16	737.68	0.63
SVM	2.55	674.93	<0.01
RT	0.26	686.74	0.19
Reg1	1.47	639.67	<0.01
Reg2	0.62	548.72	0.01
PT–JPL	0.36	847.29	0.18
PM–Yuan	0.78	572.72	<0.01
PM–MOD16	−0.04	536.09	0.88

a and b indicate the slope and intercept of linear regression equations between annual mean ET (mm yr^{-1}) and year.

Energy partitioning was the most important factor in determining the magnitude and fraction of ET components. Both the PT–JPL and PM–Yuan models used the Beer–Lambert law to exponentially partition net radiation between the canopy and the soil surface. Net radiation is partitioned between the canopy and soil surface based on the vegetation cover fraction in the PM–MOD16 model, and MOD15A2 FPAR (the Fraction of Absorbed Photosynthetically Active Radiation) was used as a surrogate for vegetation cover fraction. Moreover, PM–MOD16 also subtracts soil heat flux from the available evaporation energy. The results indicate similar spatial patterns of energy partitioning within PT–JPL and PM–Yuan models, with both differing from those of PM–MOD16 (Fig. 9). The latter simulated a large energy allocation to vegetation canopy and lower fraction to soil surface (Fig. 9). As a result of differences in energy partitioning, the contributions of the components to the total ET differed substantially among the three models. PM–Yuan model separates ET into vegetation canopy transpiration and soil evaporation; thus, the ratio of ET_s to ET was larger than those of PM–MOD16 and PT–JPL models (Fig. 9). The fraction for ET_i of the PM–MOD16 was almost double that of the PT–JPL model.

3.3. Differences in environmental regulations of the ET models

ET was regulated by many factors, including solar radiation, surface moisture, and air temperature. In this study, several models, including ANN, SVM, Reg2, PT–JPL and PM–Yuan showed strongly positive correlations between ET and solar radiation over south China, and a positive correlation with water availability over north China (Fig. 10), which matched spatial patterns of dryness as it increases from south to north in China. Air temperature regulated the variability in ET in only some of the models. In the Reg1 model, air temperature drove the ET variations in the northeast, on the Tibetan plateau and in the central regions of China (Fig. 10). Only a few weak positive temperature contributions to ET were found over the cold areas of the Tibetan plateau and Qinghai Province within RT, PT–JPL and PM–Yuan. On the other hand, vegetation plays an important role in regulating ecosystem ET in most ET models in the current study. Reg1 and Reg2 positively correlated vegetation with ET over most regions (Fig. 10). PM–Yuan and PM–MOD16 showed positive correlations of LAI with ET except in parts of Tibet and Qinghai province (Fig. 10).

Differences in model-dominated variables resulted in significant differences in the interannual variation of ET. Obvious spatial trends in long-term ET were substantially different over the 28 years. Fig. 10 shows that the key meteorological variables related with ET such as radiation, atmospheric humidity and air temperature all changed significantly over much of China. Correlation analyses showed strong positive relationships between ET estimates and NDVI, T_a and R_n within the Reg1 model. These three environmental variables increased strongly between 1982 and 2009 (Fig. 11), which resulted in interannual variations in ET. Over northeast China, ET estimations were significantly correlated with air humidity in four models (PT–JPL, Reg2, RT and ANN), such that decreased air humidity led to consistent ET changes in these four models (Fig. 11).

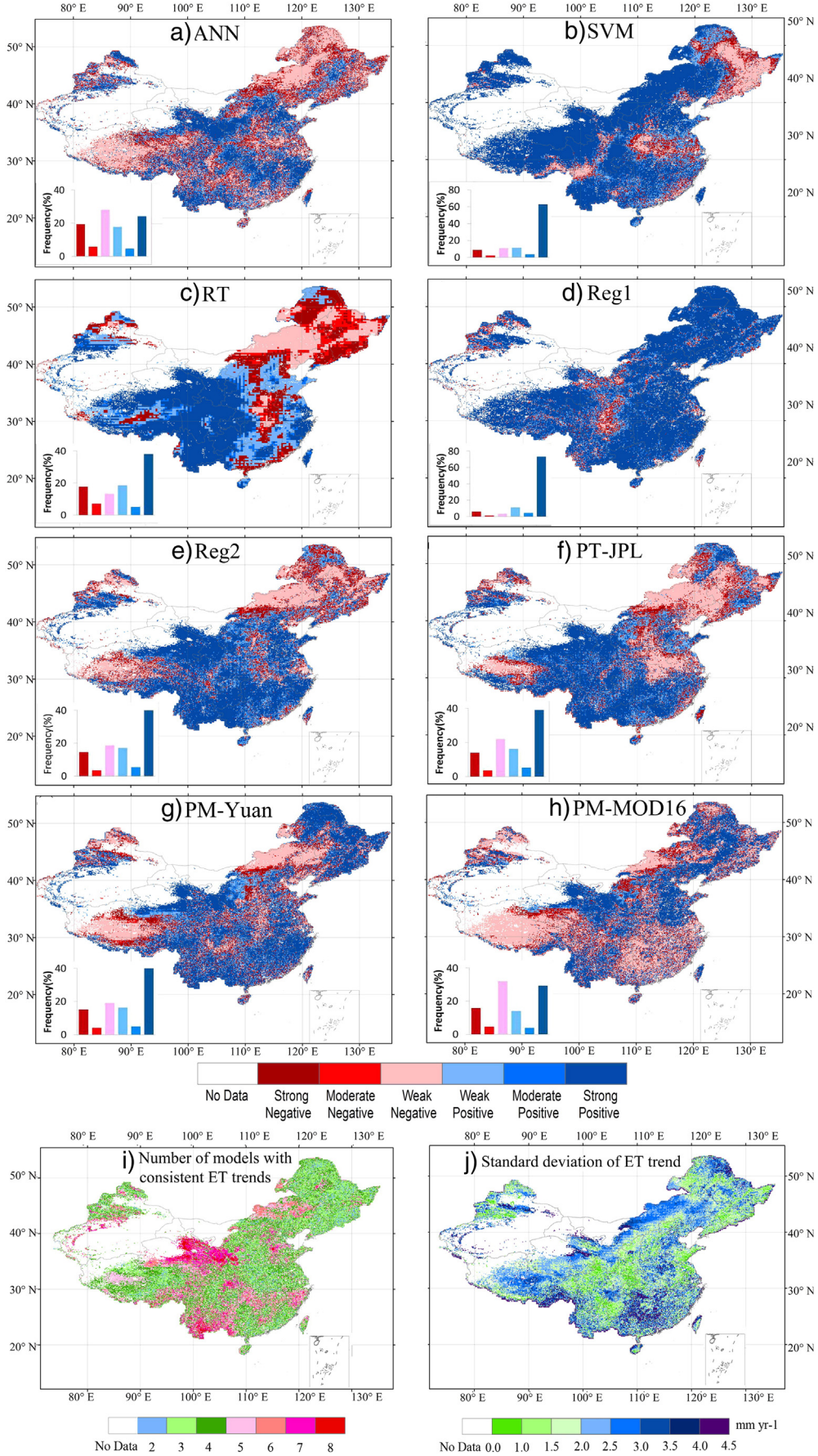

Fig. 8. Spatial patterns of long-term ET trends of eight models from 1982 to 2009 (a–h), number of models with consistent ET trend (i) and standard deviation of changed magnitude (mm yr^{-1}) (j). The inside panels indicate the fraction of various change trends.

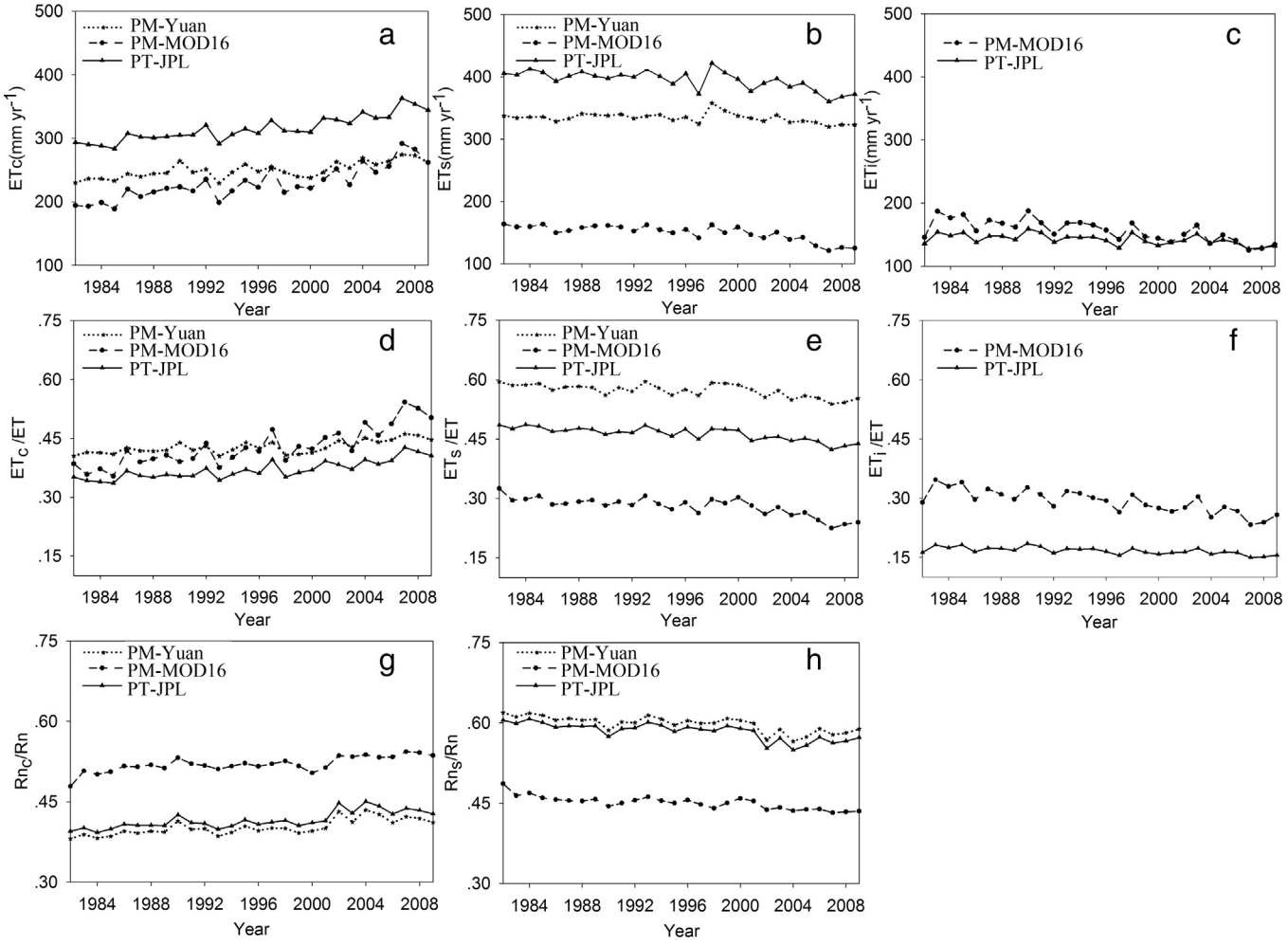

Fig. 9. The interannual variability on magnitude and fractions of ET components and energy component fraction at the three process-based models. (a–c) show the interannual of canopy transpiration (ET_c), soil evaporation (ET_s) and intercepted surface evaporation (ET_i); (d–f) show the ratio of ET_c, ET_s and ET_i to total ecosystem ET; (g–h) show the energy ratio to canopy (Rn_c) and soil surface (Rn_s).

4. Discussion

4.1. Model performance

The objective of this paper was to evaluate eight ET models over China based on EC measurements. Three machine learning methods (i.e., ANN, RT and SVM) were included in the comparison and had the lowest model performances. These three methods build functional relationships between the response (in this case ET) and predictor variables, while ignoring explicit biophysical mechanisms. These machine learning methods construct an ET algorithm based only on data and are typically data-limited. This "data limitation" refers to the quantity, quality, and representativeness of the training dataset (Jung et al., 2011). Our analyses found that the ability of ANN, SVM and RT depended highly on the size of the training dataset (Table 1). Previous studies have supported our conclusion and highlighted that statistical models are confined to the data dimensions (e.g., space, time, climate, environmental behavior) in which they are trained; thus, extrapolating outside those dimensions may not be robust and may lead to large uncertainties (Fisher et al., 2009). Twenty-three EC sites are insufficient to represent the major vegetation types and climate regions of China, which was the main cause of the poor performance of the three machine learning methods.

Previous research has indicated that empirical models need recalibration to transfer to other areas (Feddes & Lenselink, 1994). Our validation results showed that the two empirical methods, Reg1 and Reg2, had a higher R^2 value and a lower RMSE. These two empirical models have been developed and validated primarily with ET data collected by AmeriFlux. Our evaluation results showed that these methods could be safely applied in China. However, our results also showed that the parameters of the empirical methods might have different combinations. This is because the environmental factors of ET are not independent, i.e., air temperature and solar radiation are closely related.

The three process-based models exhibited larger inter-model differences relative to the five empirical models, and the largest ET estimate, derived by the PT–JPL model, was 1.69 times of that of the PM–MOD16 model, which gave the smallest ET estimate. These results were unexpected because the process-based models were developed by integrating mechanistic processes. These three process-based models have been evaluated and validated globally. In this study, no efforts were made to calibrate the model parameters, and the default parameter values from the original model were used. Therefore, they were supposed to represent relatively similar and consistent regional ET simulations. The PT–JPL model has no empirically-calibrated parameters, and is therefore highly sensitive to the quality and biases of the input data. For example, Fisher et al. (2008) used SRB net radiation data from the Global Energy and Water Cycle Experiment (GEWEX) for their global product. In this study, MERRA net radiation was used to drive regional ET simulations. Comparison of the GEWEX and MERRA R_n showed that the latter significantly overestimated R_n at 23 EC sites (Fig. 12a), and aggregated over the whole of China, MERRA R_n was almost 2.76 times the GEWEX value; subsequently, PT–JPL, as driven by MERRA R_n

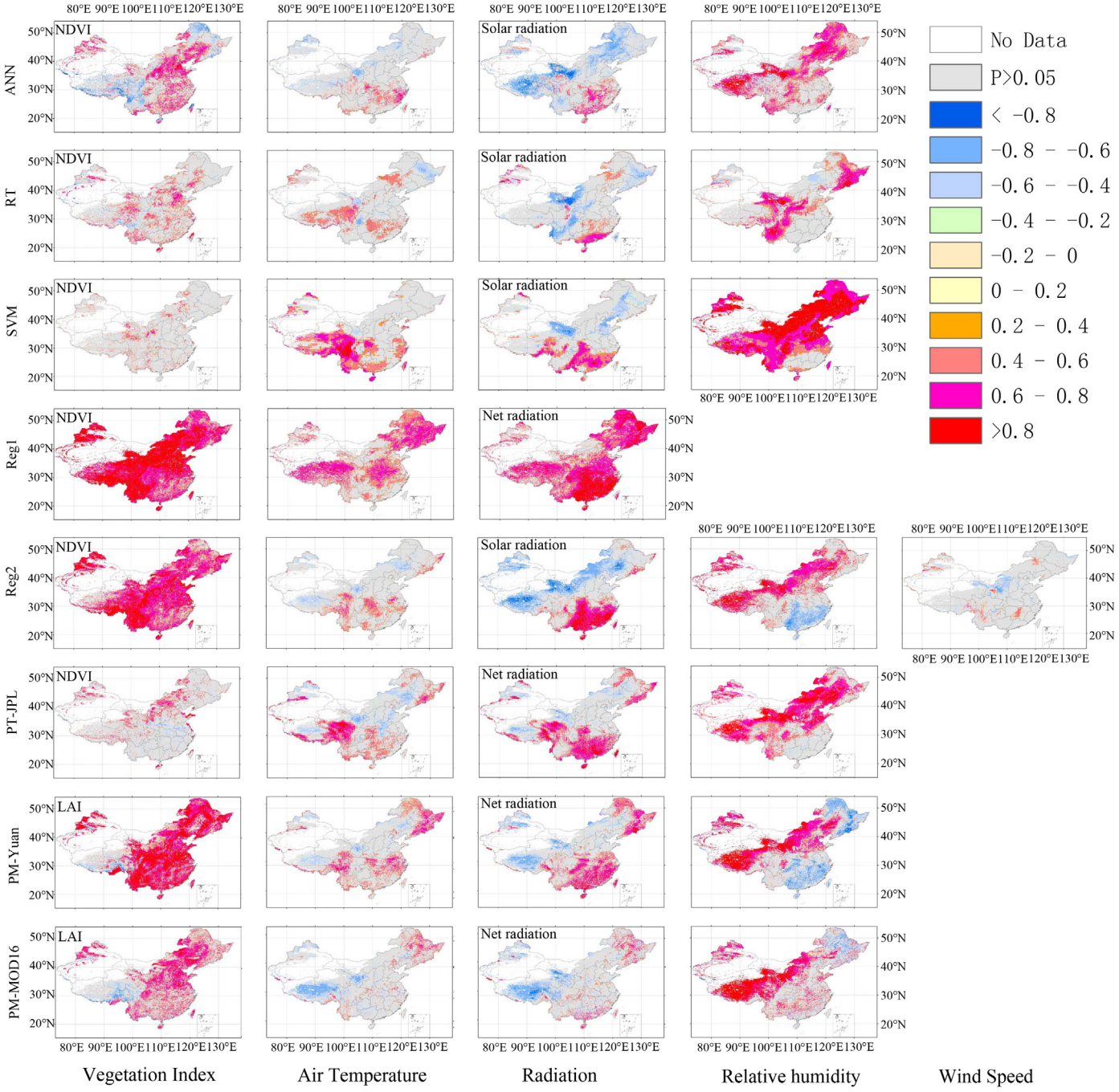

Fig. 10. Spatial patterns of coefficient of determination (R) between ET estimations and environmental variables. The grids with insignificant correlations were marked in gray, and other colors indicate significant correlations ($p < 0.05$).

also produced overestimates. In contrast, PM–Yuan and PM–MOD16 were developed and calibrated based on DAO and MERRA reanalysis datasets, and both of them used the Goddard Earth Observing System (GEOS) Data Assimilation System (Mu et al., 2011; Yuan et al., 2010). Therefore, we did not find the anomalously high ET overestimation in this study compared with applications of the original models. These results imply that, for high accuracy ET, either the forcing data to the ET algorithms must be biased-adjusted or that the models must be calibrated to correct for input biases.

Moreover, previous studies have suggested that the mismatch between ET estimates based on remote sensing and tower observations makes process-based model calibration challenging. McCabe and Wood (2006) investigated the impact of errors in ET retrievals that resulted from the scale of the remote sensing inputs, and showed that the errors in large regional ET estimates based on tower observations were caused by land surface heterogeneity. Currently, only EC measurements can be used for large scale direct ET validation, so scaling beyond an EC footprint is largely unknown (Vinukollu et al., 2011). Therefore, additional work is required to improve the model calibration and validation. For example, some studies are using inferred evaporation as calculated by climatological precipitation and basin discharge to investigate model performance (Jung et al., 2010; Vinukollu et al., 2011).

All three process-based models developed algorithms to quantify the variation in the components of ET. However, no sub-component was validated because of lack of measurements. Stable isotope and sap flow measurements can be used to partition plant transpiration and soil evaporation (Brunel, Walker, Dighton, & Monteny, 1997; Swanson, 1994), but only a few measurements were used to validate the ET models

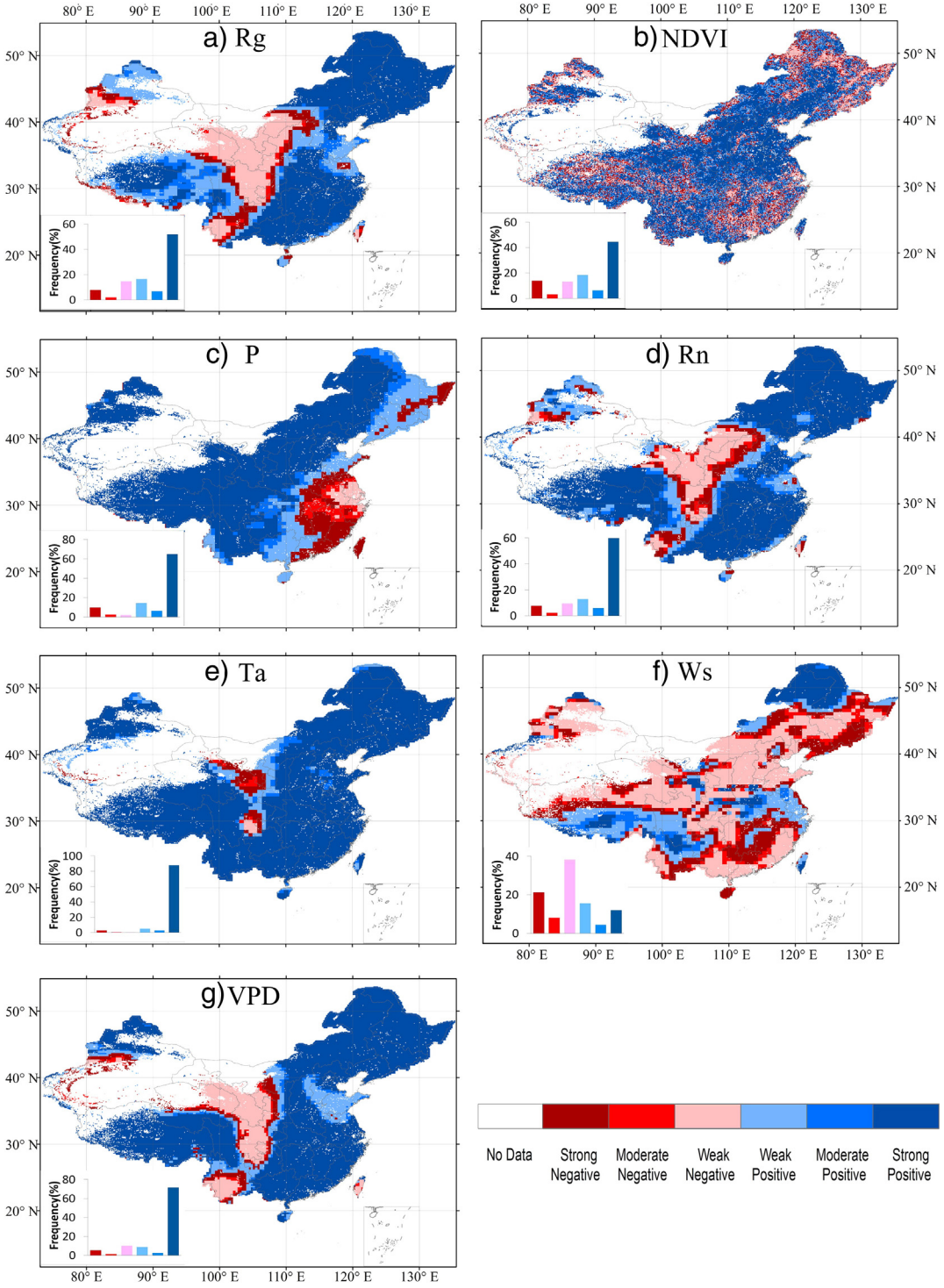

Fig. 11. Spatial patterns of long-term variation trends in annual mean total radiation (R_g), normalized difference vegetation index (NDVI), atmosphere pressure (P), net radiation (R_n), air temperature (T_a), wind speed (W_s) and vapor pressure deficit (VPD) over the terrestrial area of China.

in this study. Among the three process-based models in this study, the accuracy of ET sub-components was examined only for PT–JPL and only at three sites (Fisher et al., 2008). Therefore, it is necessary to collect ET component measurements at more sites and over wider geographical regions for more thorough model validation.

4.2. Differences in environmental regulation of ET models

Water and energy have long been considered as the most important variables driving ecosystem evapotranspiration at both hydroclimatologic and agronomic scales of space and time (Donohue, Roderick, & McVicar, 2007). In this study, most of the models found strong correlations between ET simulations and the radiation over the cloudy south China and the humidity over the dry north of China. These results were consistent with previous studies. For example, McVicar et al. (2012) mapped the global distribution of areas where ET was energy-limited or water-limited based on the long-term ratio of annual average precipitation to potential ET, and the results indicated that energy and water control ET in southern and northern China, respectively. In particular, Reg1 generated positive correlations between

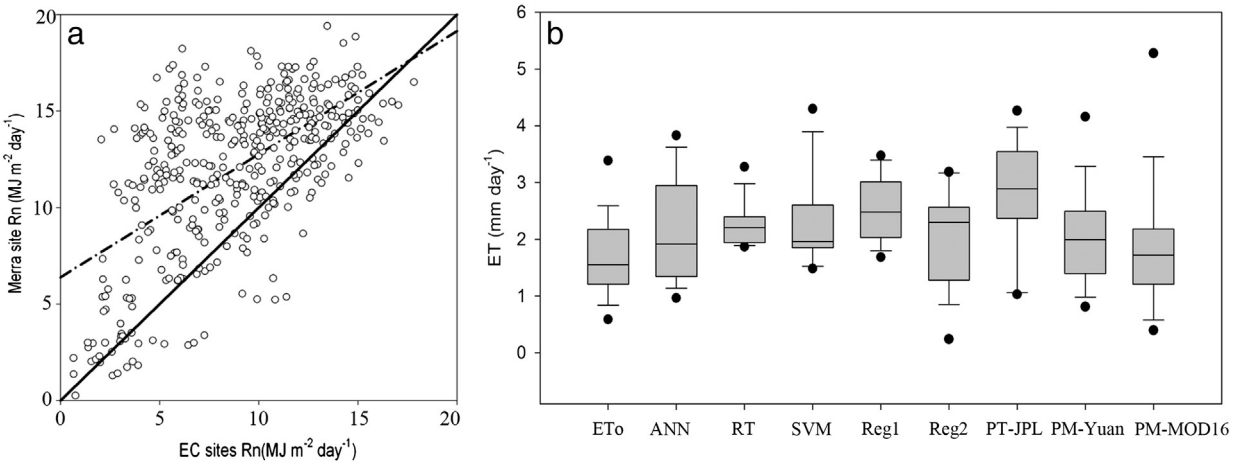

Fig. 12. Comparison of observed R_n at EC sites with MERRA production (a). The solid line is 1:1 line and the short dash line is regression line. Comparison of observed ET at EC sites with estimates driven by MERRA data (b).

radiation and ET simulations over south and north China (Fig. 10) because it does not integrate water limitation, which resulted in the same trend of interannual variability of ET as radiation significantly increased ET over most of China (Figs. 7, 11).

Wind speed is widely recognized as a critical meteorological variable that varies with the temporal and spatial changes in ET (Sellers et al., 1997). However, most of the ET models were formulated not to include wind speed as a driver because wind speed is not globally observable. Other environmental variables can be derived from satellite datasets, but wind speed data must come from a reanalysis dataset, which would reduce the consistency and accuracy of the model forcing data. In this study, only the Reg2 model required wind speed as a model input. A recent study quantified the sensitivity of rates of evaporative demand to changes in wind speed and found that wind speed contributed substantially to declining evaporation rates (McVicar et al., 2012; Sheffield, Wood, & Roderick, 2012). Our results showed significant interannual variation in wind speed over most of the regions (Fig. 11), therefore ignoring wind speed may create large errors in long-term changes in ET.

Temperature is another important meteorological factor influencing evapotranspiration because it can be used as a surrogate for atmospheric demand (Jung et al., 2010). Many ET models were developed from temperature based models (Hamon, 1961; Kharrufa, 1985; Thornthwaite, 1948). All of the models in this study integrated the impact of temperature on ET. Our results showed that air temperature dominated the ET variation in the northeast and the Tibetan plateau of China for the most of the models (Fig. 10). This was consistent with previous studies. For example, one previous global study found temperature to exert significant control over ET and be generally positively related to ET in high latitude and cold areas (Iwasaki, Saito, Kuwao, Maximov, & Hasegawa, 2009). Therefore, understanding the response of evapotranspiration to global temperature change is very important so that future ecosystem water cycles can be predicted for those regions.

5. Summary

In this study, we compared eight evapotranspiration models, including five empirical models and three process-based models, based on 23 eddy covariance sites in China. The results showed that the eight models explained between 61 and 80% of the variability in ET. The process-based models performed better than the five empirical models. The empirical models were strongly dependent on the training datasets. Regionally, although all eight models indicated similar spatial patterns, with decreased ET from southeast to northwest, there were substantial differences in the magnitude of ET. Mean annual ET estimates ranged from 535 to 852 mm yr^{-1}, and models differed more in tropical and humid areas. Four of the eight models (SVM, Reg1, Reg2 and PM–Yuan) showed significant increases in ET from 1982 to 2009, but the other models (RT, PT–JPL and PM–MOD16) presented constant long-term values or decreasing trends. The differences in model structures and their dominant variables were the major cause of ET simulations at both site and region scales. The three process-based models applied different energy partition equations, resulting in substantial differences in the simulations of ET components. Overall, the dominant driving variables differed among the eight models, which caused significant differences in their interannual variability. Our results showed that it is necessary to examine model structure to improve the ET component estimations and critical model parameters.

Acknowledgments

This study was supported by the National Science Foundation for Excellent Young Scholars of China (41322005), the National High Technology Research and Development Program of China (863 Program) (2013AA122003), National Natural Science Foundation of China (41201078), Program for New Century Excellent Talents in University (NCET-12-0060), One Hundred People Plan of the Chinese Academy of Sciences, the National Basic Research Program of China (2010CB833504 and 2012CB955302), the National Natural Science Foundation of China (40830957) and Fundamental Research Funds for the Central Universities. We thank the Coordinated Observations and Integrated Research over Arid and Semi-arid China (COIRAS) for providing the eddy covariance flux data. We also acknowledge all the principal investigators, AsiaFlux and ChinaFlux for their volunteer contribution for data distribution. JBF contributed to this paper at the Jet Propulsion Laboratory, California Institute of Technology, under a contract with the National Aeronautics and Space Administration. We acknowledge Jun Asanuma, Shiping Chen, Minoru Gamo, Jianping Huang, Shijie Han, Huizhi Liu, Shaomin Liu, Takahisa Maeda, Takeshi Ohta, Runyuan Wang, Guoyi Zhou and Xinquan Zhao for using their monitoring data.

References

Bonan, G. B. (2008). *Ecological climatology: Concepts and applications*. UK: The United Kingdom at the University Press, Cambridge, 31.

Bormann, H. (2010). Sensitivity analysis of 18 different potential evapotranspiration models to observed climatic change at German climate stations. *Climatic Change, 104*, 729–753.

Brunel, J. P., Walker, G. R., Dighton, J. C., & Monteny, B. (1997). Use of stable isotopes of water to determine the origin of water used by the vegetation and to partition evapotranspiration: A case study from HAPEX-Sahel. *Journal of Hydrology, 188–189*, 466–481.

Chen, J. Y., & Bosilovich, M. G. (2008). A preliminary study of global water and energy cycles in a NASA reanalysis system. *20th Conference on Climate Variability and Change*.

Cleugh, H. A., Leuning, R., Mu, Q., & Running, S. W. (2007). Regional evaporation estimates from flux tower and MODIS satellite data. *Remote Sensing of Environment*, *106*, 285–304.

Dawson, C. W., & Wilby, R. (1998). An artificial neural network approach to rainfall-runoff modelling. *Hydrological Sciences Journal*, *43*, 47–66.

Dirmeyer, P. A., Gao, X., Zhao, M., Guo, Z., Oki, T., & Hanasaki, N. (2006). GSWP-2: Multimodel analysis and implications for our perception of the land surface. *Bulletin of the American Meteorological Society*, *87*, 1381–1397.

Donohue, R. J., Roderick, M. L., & McVicar, T. R. (2007). On the importance of including vegetation dynamics in Budyko's hydrological model. *Hydrology and Earth System Sciences*, *11*, 983–995.

Drake, J. M., Randin, C., & Guisan, A. (2006). Modelling ecological niches with support vector machines. *Journal of Applied Ecology*, *43*, 424–432.

Feddes, R. A., & Lenselink, K. J. (1994). *Drainage principles and practices*. Holland: International Institute for Land Reclamation and Improvement, 146.

Fisher, J. B., Malhi, Y., Bonal, D., Darocha, H. R., Araujo, A.D., Gamo, M., et al. (2009). The land–atmosphere water flux in the tropics. *Global Change Biology*, *15*, 2694–2714.

Fisher, J. B., Tu, K. P., & Baldocchi, D.D. (2008). Global estimates of the land–atmosphere water flux based on monthly AVHRR and ISLSCP-II data, validated at 16 FLUXNET sites. *Remote Sensing of Environment*, *112*, 901–919.

Foken, T. (2008). The energy balance closure problem: An overview. *Ecological Applications*, *18*, 1351–1367.

Friedl, M.A. (1996). Relationships among remotely sensed data, surface energy balance, and area-averaged fluxes over partially vegetated land surfaces. *Journal of Applied Meteorology*, *35*, 2091–2103.

Gash, J. H. C. (1987). An analytical framework for extrapolating evaporation measurements by remote sensing surface temperature. *International Journal of Remote Sensing*, *8*, 1245–1249.

Global Modeling and Assimilation Office (2004). *File specification for GEOSDAS gridded output version 5.3, report*. Greenbelt, Md: NASA Goddard Space Flight Cent.

Guan, X., Huang, J., Guo, N., Bi, J., & Wang, G. (2009). Variability of soil moisture and its relationship with surface albedo and soil thermal parameters over the Loess Plateau. *Advances in Atmospheric Sciences*, *26*(9), 692–700.

Gupta, H. V., Kling, H., Yilmaz, K. K., & Martinez, G. F. (2009). Decomposition of the mean squared error and NSE performance criteria: Implications for improving hydrological modeling. *Journal of Hydrology*, *377*, 80–91.

Haddeland, I., Clark, D. B., Franssen, W., Ludwig, F., Voß, F., Arnell, N. W., et al. (2011). Multimodel estimate of the global terrestrial water balance: Setup and first results. *Journal of Hydrometeorology*, *12*, 869–884.

Hamon, W. R. (1961). Estimating potential evapotranspiration. *Journal of the Hydraulics Division, Proceedings of the American Society of Civil Engineers*, *87*, 107–120.

Holben, B. N. (1986). Characteristics of maximum-value composite images from temporal AVHRR data. *International Journal of Remote Sensing*, *7*, 1417–1434.

Huang, J. P., Guan, X., & Ji, F. (2012). Enhanced cold-season warming in semi-arid regions, Atmos. *Journal of Chemical Physics*, *12*, 5391–5398.

Huang, J. P., Zhang, W., Zuo, J., Bi, J., Shi, J., Wang, X., et al. (2008). An overview of the semi-arid climate and environment research observatory over the Loess Plateau. *Advances in Atmospheric Sciences*, *25*(6), 1–16.

Iwasaki, H., Saito, H., Kuwao, K., Maximov, T. C., & Hasegawa, S. (2009). Forest decline caused by high soil water conditions in a permafrost region. *Hydrology and Earth System Sciences*, *6*, 6087–6105.

Jiménez, C., Prigent, C., & Aires, F. (2009). Toward an estimation of global land surface heat fluxes from multisatellite observations. *Journal of Geophysical Research*, *114*, D06305. http://dx.doi.org/10.1029/2008JD011392.

Jiménez, C., Prigent, C., Mueller, B., Seneviratne, S. I., McCabe, M. F., Wood, E. F., et al. (2011). Global intercomparison of 12 land surface heat flux estimates. *Journal of Geophysical Research*, *116*, D02102. http://dx.doi.org/10.1029/2010JD014545.

June, T., Evans, J. R., & Farquhar, G. D. (2004). A simple new equation for the reversible temperature dependence of photosynthetic electron transport: a study on soybean leaf. *Functional Plant Biology*, *31*, 275–283.

Jung, M., Reichstein, M., Ciais, P., Seneviratne, S. I., Sheffield, J., Goulden, M. L., et al. (2010). Recent decline in the global land evapotranspiration trend due to limited moisture supply. *Nature*, *467*, 951–954.

Jung, M., Reichstein, M., Margolis, H. A., Cescatti, A., Richardson, A.D., Arain, M.A., et al. (2011). Global patterns of land–atmosphere fluxes of carbon dioxide, latent heat, and sensible heat derived from eddy covariance, satellite, and meteorological observations. *Journal of Geophysical Research*, *116*, G00J07. http://dx.doi.org/10.1029/2010JG001566.

Keane, R. E., Ryan, K. C., Veblen, T. T., Allen, C. D., Logan, J., & Hawkes, B. (2002). Cascading effects of fire exclusion in Rocky Mountain ecosystems: A literature review. *USDA forest service general technical report RMRS-GTR-91* (24 pp.).

Kennedy, A.D., Dong, X. Q., Xi, B. K., Xie, S.C., Zhang, Y. Y., & Chen, J. (2011). A comparison of MERRA and NARR reanalyses with the DOE ARM SGP data. *Journal of Climate*, *24*, 4541–4557.

Kharrufa, N. S. (1985). Simplified equation for evapotranspiration in arid regions. *Hydrologie Sonderheft*, *5*(1), 39–47.

Kustas, W. P., & Norman, J. M. (1996). Use of remote sensing for evapotranspiration monitoring over land surfaces. *Hydrological Sciences*, *41*, 495–516.

Lettenmaier, D. P., & Famiglietti, J. S. (2006). Water from on high. *Nature*, *444*, 562–563.

Li, S., Kang, S., Li, F., & Zhang, L. (2008). Evapotranspiration and crop coefficient of spring maize with plastic mulch using eddy covariance in northwest China. *Agricultural Water Management*, *95*, 1214–1222.

Li, X., Li, X. W., Li, Z. Y., Ma, M. G., Wang, J., Xiao, Q., et al. (2009). Watershed allied telemetry experimental research. *Journal of Geophysical Research*, *114*, D22103. http://dx.doi.org/10.1029/2008JD011590.

Liang, S. L., Li, X. W., & Wang, J.D. (2012). *Advanced remote sensing: Terrestrial information extraction and applications*. UK: Academic Press, 506.

McCabe, M. F., & Wood, E. F. (2006). Scale influences on the remote estimation of evapotranspiration using multiple satellite sensors. *Remote Sensing of Environment*, *105*, 271–285.

McVicar, T. R., & Jupp, D. L. B. (1998). The current and potential operational uses of remote sensing to aid decisions on drought exceptional circumstances in Australia, a review. *Agricultural Systems*, *57*, 399–468.

McVicar, T. R., Roderick, M. L., Donohue, R. J., Li, L. T., Van Niel, T. G., Thomas, A., et al. (2012). Global review and synthesis of trends in observed terrestrial near-surface wind speeds: Implications for evaporation. *Journal of Hydrology*, *416–417*, 182–205.

Meyer, W. (1999). Standard reference evaporation calculation for inland, south eastern Australia. *Technical report.* , *Vol. 35/98*, . Adelaide, South Australia: CSIRO Land and Water.

Miralles, D.G., Holmes, T. R. H., De Jeu, R. A.M., Gash, J. H., Meesters, A. G. C. A., & Dolman, A. J. (2011). Global land-surface evaporation estimated from satellite-based observations. *Hydrology and Earth System Sciences Discussions*, *15*, 453–469.

Mohandes, M.A., Halawani, T. O., Rehman, S., & Hussain, A. A. (2004). Support vector machines for wind speed prediction. *Renewable Energy*, *29*, 939–947.

Monteith, J. L. (1965). Evaporation and the environment. *Symposium of the Society of Exploratory Biology*, *19*, 205–234.

Mu, Q., Heinsch, F. A., Zhao, M., & Running, S. W. (2007). Development of a global evapotranspiration algorithm based on MODIS and global meteorology data. *Remote Sensing of Environment*, *111*, 519–536.

Mu, Q., Zhao, M., & Running, S. W. (2011). Improvements to a MODIS global terrestrial evapotranspiration algorithm. *Remote Sensing of Environment*, *115*, 1781–1800.

Mueller, B., Seneviratne, S. I., Jiménez, C., Corti, T., Hirschi, M., Balsamo, G., et al. (2011). Evaluation of global observations-based evapotranspiration datasets and IPCC AR4 simulations. *Geophysical Research Letters*, *38*, L06402. http://dx.doi.org/10.1029/2010GL-46230.

Myneni, R. B., Hoffman, S., Knyazikhin, Y., Privette, J. L., Glassy, J., Tian, Y., et al. (2002). Global products of vegetation leaf area and fraction absorbed PAR from year one of MODIS data. *Remote Sensing of Environment*, *83*, 214–231.

Myneni, R. B., Nemani, R. R., & Running, S. W. (1997). Estimation of global leaf area index and absorbed par using radiative transfer models. *IEEE Transactions on Geoscience and Remote Sensing*, *36*, 1380–1393.

Papale, D., & Valentini, A. (2003). A new assessment of European forests carbon exchanges by eddy fluxes and artificial neural network spatialization. *Global Change Biology*, *9*, 525–535.

Priestley, C. H. B., & Taylor, R. J. (1972). On the assessment of surface heat flux and evaporation using large-scale parameters. *Monthly Weather Review*, *100*, 81–92.

Raupach, M. R. (2001). Combination theory and equilibrium evaporation. *Quarterly Journal of the Royal Meteorological Society*, *127*, 1149–1181.

Ruimy, A., Kergoat, L., Bondeau, A., & intercomparison, T. p. N. m (1999). Comparing global models of terrestrial net primary productivity (NPP): Analysis of differences in light absorption and light-use efficiency. *Global Change Biology*, *5*, 56–64.

Rumelhart, D. E., Hinton, G. E., & Williams, R. J. (1986). Learning representations by back-propagating errors. *Nature*, *323*, 533–536.

Sellers, P. J., Dichinson, R. E., Randall, D. A., Betts, A. K., Hall, F. G., Berry, J. A., et al. (1997). Modeling the exchange of energy water and carbon between continents and the atmosphere. *Science*, *275*, 502–509.

Sheffield, J., Wood, E. F., & Roderick, M. L. (2012). Little change in global drought over the past 60 years. *Nature*, *491*, 435–438.

Su, H., McCabe, M. F., Wood, E. F., Su, Z., & Prueger, J. H. (2005). Modeling evapotranspiration during SMACEX: Comparing two approaches for local- and regional-scale prediction. *Journal of Hydrometeorology-Special Section*, *6*, 910–922.

Swanson, R. H. (1994). Significant historical developments in thermal methods for measuring sap flow in trees. *Agricultural and Forest Meteorology*, *72*(1–2), 113–132.

Thornthwaite, C. W. (1948). An approach toward a rational classification of climate. *Geographical Review*, *38*, 55–94.

Tripathi, S., Srinivas, V. V., & Nanjundiah, R. S. (2006). Downscaling of precipitation for climate change scenarios: A support vector machine approach. *Journal of Hydrology*, *330*, 621–640.

Vapnik, V. N. (1998). *Statistical learning theory*. New York: Wiley, 401–441.

Vinukollu, R. K., Meynadier, R., Sheffield, J., & Wood, E. F. (2011). Multi-model, multi-sensor estimates of global evapotranspiration: Climatology, uncertainties and trends. *Hydrological Processes*, *25*, 3993–4010.

Vinukollu, R. K., Wood, E. F., Ferguson, C. R., & Fisher, J. B. (2011). Global estimates of evapotranspiration for climate studies using multi-sensor remote sensing data: Evaluation of three process-based approaches. *Remote Sensing of Environment*, *115*, 801–823.

Wang, K. C., & Dickinson, R. E. (2012). A review of global terrestrial evapotranspiration: Observation, modeling, climatology, and climatic variability. *Reviews of Geophysics*, *50*, RG2005. http://dx.doi.org/10.1029/2011RG000373.

Wang, K. C., Dickinson, R. E., Wild, M., & Liang, S. (2010). Evidence for decadal variation in global terrestrial evapotranspiration between 1982 and 2002: 1. Model development. *Journal of Geophysical Research*, *115*, D20112. http://dx.doi.org/10.1029/2009JD013671.

Wang, K. C., & Liang, S. (2008). An improved method for estimating global evapotranspiration based on satellite estimation of surface net radiation, vegetation index, temperature, and soil moisture. *Journal of Hydrometeorology*, *9*(4), 712–727.

Wang, K. C., Wang, P., Li, Z., Cribb, M., & Sparrow, M. (2007). A simple method to estimate actual evapotranspiration from a combination of net radiation, vegetation index, and temperature. *Journal of Geophysical Research*, *112*, D15107. http://dx.doi.org/10.1029/2006JD008351.

Werth, D., & Avissar, R. (2004). The regional evapotranspiration of the Amazon. *Journal of Hydrometeorology*, *5*, 100–109.

Wilson, K. B., Hanson, P. J., Mulholland, P. J., Baldocchi, D.D., & Wullschleger, S. D. (2001). A comparison of methods for determining forest evapotranspiration and its components: Sap-flow, soil water budget, eddy covariance and catchment water balance. *Agricultural and Forest Meteorology*, *106*, 153–168.

Xiao, J., Zhuang, Q., Law, B. E., Chen, J., Baldocchi, D.D., Cook, D. R., et al. (2010). A continuous measure of gross primary production for the conterminous United States derived from MODIS and AmeriFlux data. *Remote Sensing of Environment*, *114*, 576–591.

Yang, F. H., Ichii, K., White, M.A., Hashimoto, H., Michaelis, A.R., Votava, P., et al. (2007). Developing a continental-scale measure of gross primary production by combining MODIS and AmeriFlux data through support vector machine approach. *Remote Sensing of Environment*, *110*, 109–122.

Yang, F. H., White, M.A., Michaelis, A.R., Ichii, K., Hashimoto, H., Votava, P., et al. (2006). Prediction of continental-scale evapotranspiration by combining MODIS and AmeriFlux data through support vector machine. *IEEE Transactions on Geoscience and Remote Sensing*, *44*, 3452–3461.

Yuan, W. P., Liu, S., Yu, G., Bonnefond, J. -M., Chen, J., Davis, K., et al. (2010). Global estimates of evapotranspiration and gross primary production based on MODIS and global meteorology data. *Remote Sensing of Environment*, *114*, 1416–1431.

Zhang, B., Kang, S., Li, F., & Zhang, L. (2008). Comparison of three evapotranspiration models to Bowen ratio-energy balance method for a vineyard in an arid desert region of northwest China. *Agricultural and Forest Meteorology*, *148*, 1629–1640.

Zhang, K., Kimball, J. S., Hogg, E. H., Zhao, M., Oechel, W. C., Cassano, J. J., et al. (2008). Satellite-based model detection of recent climate-driven changes in northern high-latitude vegetation productivity. *Journal of Geophysical Research*, *113*, G03033. http://dx.doi.org/10.1029/2007JG000621.

Zhang, K., Kimball, J. S., Mu, Q. Z., Jones, L. A., Goetz, S. J., & Running, S. W. (2009). Satellite based analysis of northern ET trends and associated changes in the regional water balance from 1983 to 2005. *Journal of Hydrology*, *379*, 92–110.

Zhang, L., Wylie, B., Loveland, T., Fosnight, E., Tieszen, L. L., Ji, L., et al. (2007). Evaluation and comparison of gross primary production estimates for the Northern Great Plains grasslands. *Remote Sensing of Environment*, *106*, 173–189.

Zhang, Q., Zeng, J., & Yao, T. (2012). Interaction of aerodynamic roughness length and windflow condition and its parameterization over vegetation surface. *Chinese Science Bulletin*, *57*, 1559–1567.

Zhao, M., Heinsch, F. A., Nemani, R., & Running, S. W. (2005). Improvements of the MODIS terrestrial gross and net primary production global data set. *Remote Sensing of Environment*, *95*, 164–176.

Zhou, G. Y., Sun, G., Xu, W., Zhou, G. Y., Mcnulty, S. G., Vose, J. M., et al. (2008). Estimating forest ecosystem evapotranspiration at multiple temporal scales with a dimension analysis approach. *Journal of the American Water Resources Association*, *44*, 1–14.